

Injection and detection of electric charges at nanometer scale by Electrostatic Force Microscopy

F. Marchi^{1,2,3,*}, R. Dianoux¹, F. Comin¹ and J. Chevrier^{1,2,3}

¹ ESRF, B.P. 220, 38043 Grenoble cedex 9, France

² CNRS/LEPES, 25 avenue des Martyrs, 38042 Grenoble cedex 9, France

³ Université Joseph Fourier, B.P. 53, 38041 Grenoble cedex 9, France

*marchi@grenoble.cnrs.fr

Abstract: *AFM and related electrical probe techniques as electrostatic force microscope (EFM) can perform injection and detection of electric charges in nanostructures or oxide layer at the nanometer scale. The controllable deposition of both positive and negative localised charge is described. A basic theoretical and experimental introduction to EFM coupled with an analytical calculation of tip-surface capacitance allowed quantifying the trapped charge. We have used this quantification method to measure charge storage in oxide layer and nanostructures. The charge resolution of EFM technique working at room temperature and in control atmosphere has been estimated about 20 charges. Finally, we use this technique to inject charge and to study their behavior in confined silicon nanostructures. We found that the injection efficiency relies on the thickness of oxide layer, point it out the electric field as a key parameter in the injection mechanism. The dynamics and propagation of the deposited charges have been studied and a homogenous distribution of the charge in all the nanostructure has been observed. This observation coupled to a charge energy calculation lead to the hypothesis of a Wigner crystal formation.*

1 Introduction

Scanning Force Microscopy (SFM) provides a simultaneous map of topography and various physical forces with nanometre-scale resolution, enabling straightforward correlation of physical properties with surface morphology. Atomic force microscope (AFM) and related electrostatic force microscope (EFM) are accurate tools to perform local and non-destructive electrostatic force measurements for a wide range of characterizations as surface potential, charge distribution [1,2], dopant concentration [3] and dielectric constant [4]. EFM is also able to inject and detect localised charges in nanostructures, on or below the surface. This ability have been used to study the distribution of trapped charges in wide range of samples as: Si or Co nanocrystal [5,6,7] embedded in an oxide film, oxide layers deposited on a conductive substrate [8] and even in individual quantum dots [9,10]. As the dimensions of electronic devices are scaled-down, EFM is becoming a technique of choice to study the influence of localised charges on

Coulomb blockade [11, 12] and electrons tunneling [13, 14] phenomena when nanometer dimensions are involved. Like these future devices as SET [15] or multiple-tunnel junction devices [16,17] will work at room temperature, their electronic properties have to be characterised in ambient condition, this implies a well understanding of the EFM capabilities at room temperature in term of spatial and charge resolution. In the present paper, we address this last point in the first part after a theoretical and experimental introduction of the EFM technique. The second part deals with the modeling of tip-surface capacitance in order to quantify trapped charge from EFM phase shift measurement. In the last part, we used EFM in image mode in control environment at room temperature, to study space-time behavior of electric charge in different silicon nanostructures supported on an oxide layer, after carrier injection with metallic AFM tip. The major issues of these experiments are to determine the influence of the oxide layer thickness in injection mechanism, to localise the trapped charges and finally to characterise the distribution and dynamics of charges in these Si nanostructures.

2 Injection procedure of electric charge

A conductive AFM tip can be used as a nano-tool to inject electric charges. Figure 1 describes this injection procedure. The charge injection is achieved by positioning the AFM tip above a chosen point of the scan area, disengaging the feedback control of the probe, then lowering the tip toward the sample surface and finally applying for few ms a bias voltage to the tip [-10; 10]V and the sample grounded. Observing the damping of the cantilever oscillations on an oscilloscope monitored the distance between the tip and the sample: when the oscillation amplitude is fully reduced, the tip apex is in contact with the surface. This procedure leads to estimate the oscillation amplitude of the cantilever free end, peak to peak, closed to the piezoelectric extension Δz : $\Delta z = z_1 - z_2$ with z_1 the altitude where the free oscillation starts decreasing and z_2 the altitude where the oscillation is fully reduced.

This injection procedure should be carried on control dry atmosphere where the humidity rate is low to avoid local nano-oxidation process [18, 19].

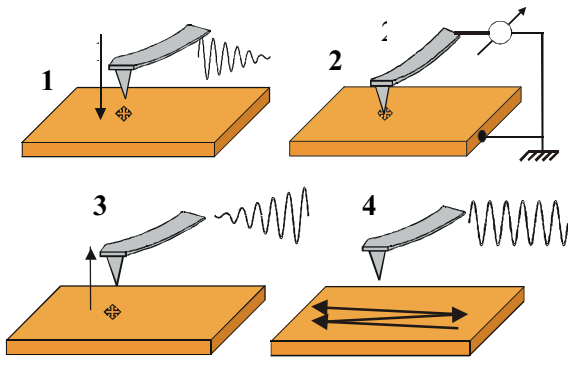


Figure 1: Injection procedure by the AFM tip. 1) the scan is stop and the tip is approaching the surface, the oscillating amplitude is decreasing until it is fully reduced; 2) Application of the tip-sample voltage; 3) tip is removed from the surface; 4) the tip is grounded and the scan restarts.

3 Theory of EFM

In the electrical AFM measurements, a double pass procedure is performed line-by-line (figure 2): (1) topography mapping in dynamic mode and (2) Electrical mapping in 'interleave' mode.

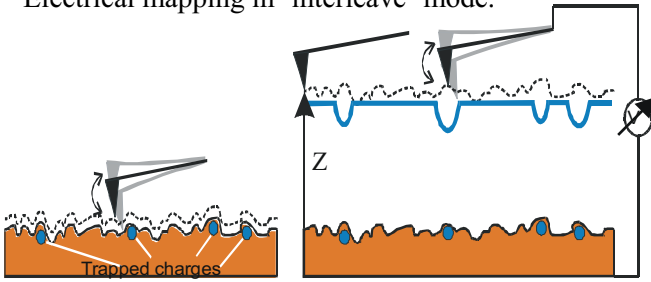


Figure 2: Double pass procedure. Left: topography scan; Right: the tip is lift at the altitude z_0 to detect the long-range forces as the electrostatic one.

Firstly the AFM probe scans the surface topography in classical dynamics mode [20] where all the types of force (long and short range) act on the AFM probe. As example, Van der Waals, capillary or chemical interactions are short-range forces while magnetic or electrostatic ones are long-range forces. In first and basic approximation, the cantilever behaviour in dynamic mode can be described as a harmonic oscillator driven mechanically by an external sinusoidal force F_{exc} closed to its resonance frequency ω_0 , probing a non-linear force potential $F_I(z)$:

$$(1) \quad z'' + \gamma z' + \omega_0^2 z = \frac{F_{exc}}{m_e} + \frac{F_I(z)}{m_e} \quad \text{with } F_{exc} = F_0 \cos \omega t$$

where z'' and z' are the second and first derivatives of tip-surface distance z in function of time t , γ is the damping factor. The non-linear force potential represents all the force acting on the tip at the nanometer scale. When the cantilever is far from

the surface, $F_I(z)$ is negligible, and equation (1) is resumed to the movement of an harmonic oscillator and has a steady solution:

$$(2) \quad z(t) = A(\omega) \cos(-\phi(\omega))$$

where $A(\omega)$ and $\phi(\omega)$ are respectively the amplitude and phase of the oscillation in function of the excitation signal, their expressions are:

$$(3) \quad (a) \quad A(\omega) = \frac{F_0}{m_e} \frac{1}{\sqrt{(\omega_0^2 - \omega^2)^2 + \gamma\omega^2}}$$

$$(b) \quad \phi(\omega) = \arctan\left(\frac{\gamma\omega}{\omega_0^2 - \omega^2}\right)$$

The amplitude expression is a Lorentzien equation with its center located at the resonance frequency ω_0 . It should be noticed that the phase has a linear dependence around ω_0 .

When the tip is closed to the surface, the tip-surface force potential $F_I(z)$ acts on the tip and disturbs the oscillating movement of the cantilever. In these conditions equation (1) can not be solve if $F_I(z)$ is unknown. Nevertheless if we consider small cantilever oscillations around the altitude z_0 and small force gradients, an approximation can be made:

$$(4) \quad F_I(z) \approx F_I(z_0) + z \frac{\partial F_I}{\partial z}(z_0)$$

In this hypothesis, equation (1) can be written as:

$$(5) \quad z'' + \gamma z' + \left(\omega_0^2 - \frac{1}{m_e} \frac{\partial F}{\partial z}(z_0)\right) z = \frac{F_{exc}}{m_e} + \frac{F_I(z_0)}{m_e}$$

The term $F_I(z_0)$ is time independent and creates a static deflection of the cantilever without interest for the rest of the mathematical treatment. However, the second term induces a variation of the resonance pulsation of the system and it can be described as a variation of the spring constant of the cantilever, given by:

$$(6) \quad \omega_m = \sqrt{\left(\omega_0^2 - \frac{1}{m_e} \frac{\partial F}{\partial z}(z_0)\right)} \approx \omega_0 \left(1 - \frac{1}{2k} \frac{\partial F}{\partial z}(z_0)\right)$$

where k is the cantilever spring constant.

For an attractive the tip-sample interactions the force gradient is positive in respect of a z increase when the tip move away from the surface. As the system stays mechanically excited at ω_0 , the interaction sets the system off its resonance and by the way the oscillating amplitude and the phase are changing. In practice to regulate in dynamics mode in air, the cantilever is excited at a fixed frequency just below its resonance frequency, the feedback loops adjusts the average tip-surface distance in order to maintain the oscillating amplitude (or the

phase) constant. In this way, the regulation is done at a constant force gradient.

After the topography pass, the electric one consists of probing only the long-range interactions and more specifically the electrostatic one. For this purpose, the AFM probe is lifted and kept at a fixed height z , above the surface, whose topography was obtained in the previous topography scan line. During this second pass, the tip is biased with respect to the sample, and probes a long range electrostatic force F_E :

$$(7) F_E(z) = \frac{1}{2} \frac{dC}{dz} (\Delta V)^2 \text{ with } \Delta V = V_t - V_s,$$

where C is the capacitance between the AFM probe and the sample, ΔV is the tip-sample potential difference with V_t and V_s are respectively tip and surface potentials.

In EFM mode, the cantilever is excited near its resonance frequency ω_0 and a dc voltage V_{EFM} is applied between the tip and the sample. If the sample surface is homogenous (no electric charges trapped), the EFM signal is regular and constant all over the surface. However if locally q electric charges are trapped, the surface potential V_s equal V_q and cause a change into the electrostatic force intensity and so into its gradient.

This gradient shift can be detected by measuring the frequency or phase shift $\Delta\omega$ and $\Delta\phi$, of the oscillating movement of the cantilever related to it [21]:

$$(8) (a) \Delta\omega = \frac{\omega_0}{2k} \frac{\partial F}{\partial z}(z_0)$$

$$(1) (b) \Delta\phi = -\frac{Q}{k} \frac{\partial F}{\partial z}(z_0) = -\frac{Q}{2k} \frac{d^2 C}{dz^2} (V_{EFM} - V_q)^2$$

where Q is the quality factor of system.

In function of the sign and value of V_{EFM} , an increase or a decrease of $\Delta\phi$ is detected above a charged region (figure 3). In the (b) configuration, V_{EFM} and V_q have the same sign but $|V_{EFM}| > |V_{qmax}|$, the force gradient increases and a bump appears in the phase signal. In (c) V_{EFM} has the opposite sign of V_q , the force gradient decreases and a hole appears in the phase signal. The (d) configuration is rare, V_{EFM} and V_q have the same sign but $|V_{EFM}| < |V_{qmax}|$, a more complex profile appears. In practise as $|V_{qmax}|$ is about few hundred mV while $|V_{EFM}|$ is set around one volt or above, this last situation is not experienced often.

To illustrate the effect of the tip polarisation, some electrons have been injected on a SiO_2 layer where they form an electron cloud. The right image of figure 4 represents the topography image where an apparent height appears due to the additional attractive force contribution of the electron cloud to the other surface forces. The left image represents the phase shift measurement for two different voltages applied to the tip: on the top V_{EFM} is set to +2V creating a bump in the image while on the bottom V_{EFM} is set to -3V creating a hole. These observations are fully described by the previous interpretation. Two main points should be

emphasized: (a) for all kind of contrast, the tip-sample interaction stays attractive in agreement of its capacitive nature; (b) the frequency or phase shift represents a difference of measurement between an uncharged and a charged region for a fixed V_{EFM} traducing an increase or a decrease of the force gradient between these two parts.

Thanks to EFM image, the localisation and the sign of trapped charges can be easily defined; nevertheless the quantification of the trapped charges is not straightforward and a lot of works have treated and still deals with this question [22, 23, 24, 25, 10].

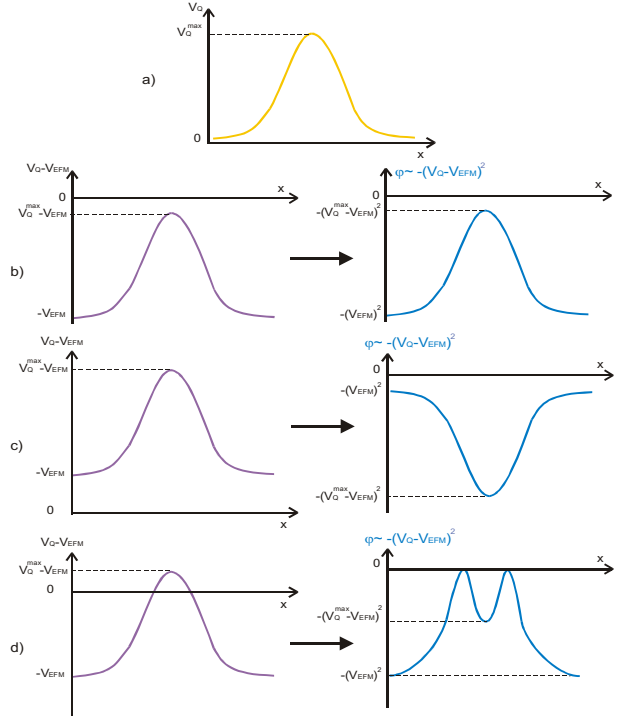


Figure 3: Sign detection of the trapped charged in function of V_{EFM} . a) surface distribution of V_q potential created by positive charge; b) $V_{EFM} > 0$ then the phase signal increases; c) $V_{EFM} < 0$ then the phase signal decreases; d) V_{EFM} has the sign as V_q but $|V_{EFM}| < |V_{qmax}|$ then a complex profil appears with a hole in the middle.

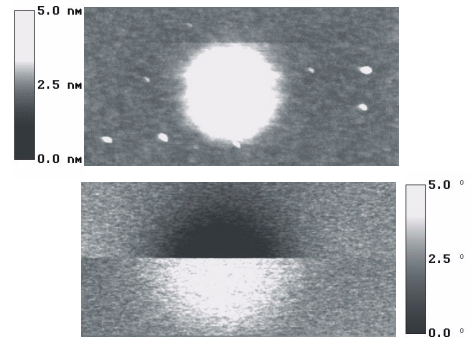


Figure 4: Topography (top) and phase (bottom) maps on a thin SiO_2 film of 25nm on Si.substrate. Scan size is $(1 \times 2) \mu m^2$. Charge injection parameters were $-10V/10s$. The phase is recorded at a lift height of 100 nm. Bottom figure, the tip voltage during lift mode is $V_{EFM} = +2V$ on the upper half of the image, then $V_{EFM} = -2V$ on the lower

half. The phase shifts jumps from -3 degrees to $+2$ degrees.

4 Quantification of the trapped charged

To deduce the surface charge q from the (8a) or (8b) equations using EFM images, the modeling of tip-sample capacitance is required because the force gradient varies with its second derivative. The capacitance of the system relies on (a) the sample characteristics as the nature and number of oxide layers deposited on the conductive bulk and its roughness, (b) the average tip-surface distance to choose the adapted surface geometry for modelling the AFM electrode. Indeed, three parts composed the AFM probe: the cantilever modelled by a plan area, the tip represented by a truncated cone [26] and the tip apex represented as a small sphere [27] or the tip and its apex by a cone [27]. Modelling the surface as a plane, each AFM part contributes to the probe-surface capacitance with a specific expression:

$$(9) \text{plane-plane: } \frac{\partial^2 C}{\partial z^2} = C''(z) = 2\varepsilon_0 \varepsilon_r \frac{S}{z^3}$$

with $\varepsilon_r \approx 1$ (air permittivity)

(10) sphere-plane:

$$C''(z) = \frac{2\pi\pi_0}{z} \left(2\left(\frac{R}{z}\right)^2 + 3\left(\frac{R}{z}\right) + \dots \right) \text{ for } z \gg R$$

$$\text{and } C''(z) = 2\varepsilon_0 \varepsilon_r \frac{R}{z^2} \text{ for } z \ll R$$

$$(11) \text{ cone-plane: } C''_{cp}(z) = -2\pi\varepsilon_0 \ln \frac{K^2}{z}$$

where K is a constant

(12) truncated cone-plane:

$$C''_{tcp}(z) \approx 2\pi\varepsilon_0 \left[\frac{R^2(2z+R)}{z^2(z+R)^2} + K^2 \left(\frac{1}{z+R} + \frac{R}{\sin\theta(z+R)^2} \right) \right]$$

To distinguish each contribution, the variation of the second derivative capacitance $C''(z_0)$ in function of the average tip-surface distance z_0 is plotted in figure 4 considering metallic probe-surface system in air. The curves were obtained by assuming that the cantilever length and width of respectively $100\mu\text{m}$ and $35\mu\text{m}$, the tip apex has a radius R of 35nm , a cone height H of $15\mu\text{m}$ with a tip-opening angle θ of 10° .

Figure 5, demonstrates that the cantilever contribution is negligible. If the total capacitance of the cantilever is large, its variation with the tip-surface distance in EFM operation is very limited, and so is the second derivative. This result has also been emphasized in Ref [28].

For typical 'interleave' distances z_0 -[50-300nm] range-, the basic plane-plane capacitor model of the tip-sample system is a relevant approximation. Indeed an adjustment of the plate

area of the plane capacitor is made, so that values of this model with the more realistic one of truncated cone-plane coincide at the chosen lift height, here 100nm . In this condition a $1.47 \times 10^4 \text{ nm}^2$ surface is found corresponding to a 140nm diameter disc. This approach leads to an effective tip area where only the tip apex augmented of a part of the cone interacts with the surface. If we apply this basic model to quantify the total charge q_t of an electron cloud in a SiO_2 layer with a thickness d on a Si bulk, the charge q located under the effective tip area induces an image charge q_0 in the Si substrate, causing a force defined by:

$$(13) F = (q+q_0)q_l / (2S\varepsilon_0)$$

where S is the effective probe area depending of the tip-surface distance z_0 and q_l is the charge image in the substrate.

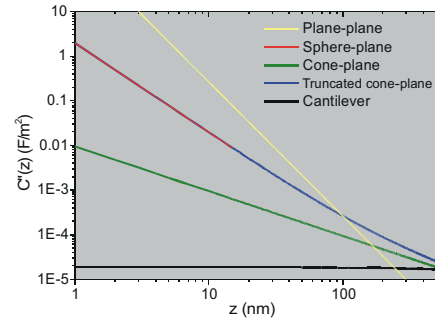


Figure 5: Second derivative of the capacitance $C''(z)$ vs. plate distance for three tip-sample models. The plate area of the plane-capacitor model has been set so as to coincide with the value of the truncated cone-plane model at a separation of 100nm .

From an electrostatic analysis of the tip-sample system modelled using the simple parallel-plate geometry, the force is found to be given by:

$$(14) F(z) = \frac{\varepsilon_0 S}{\left(z_0 + \frac{d}{\varepsilon_{\text{SiO}_2}}\right)^2} \left(V_{\text{EFM}} - \frac{qd}{\varepsilon_0 \varepsilon_{\text{SiO}_2} S} \right)^2$$

where $\varepsilon_{\text{SiO}_2}$ is the dielectric constant of the silicon oxide layer.

For $V_{\text{EFM}} = 0$, the combination of equation (8b) and the derivative of (14) leads to:

$$(15) q = \sqrt{\frac{\Delta\phi \times k \left(z_0 + \frac{d}{\varepsilon_{\text{SiO}_2}}\right) \varepsilon_0 \varepsilon_{\text{SiO}_2}^2 S}{Qd^2}}$$

where Q is the quality factor of the AFM probe

Once the q charge is known, a related charge density D can be defined and the total electron cloud can be quantify by:

$$(16) q_t = D \times A \text{ with } D = q/S$$

A is the electron cloud diameter measured at half height of the phase signal on EFM image.

Even if this simple model has been used often to quantify trapped charges in oxide layer or in embedded conductive nanostructures [5,7], this modelling tip-surface capacitance is valid only for

flat surface and EFM lift heights higher than 50nm. For smaller tip-surface distances and/or for tip-nano-structure interaction, a more complex geometry is required for reliable quantification as described in ref [10, 29].

To quantify the trapped charge, there is a second method based on the variation of the tip voltage where the direct measurement of the phase shift is not needed. The principle is to scan at a fixed altitude all the time the same line where charged and uncharged regions are included and record the phase shift (or frequency shift) in function of the tip-surface voltage V_{EFM} . By measuring the phase (or frequency) shifts on EFM image, two curves are obtained: one for the charged region and one for uncharged region (figure 6). These two curves are parabolic, which confirms a proportional interaction variation with V_{EFM}^2 but their minimum are not reached when V_{EFM} equalled zero. On the uncharged region, this minimum shift is due to the potential contact V_C between the W_2C tip and the silicon surface. In this case, the phase shift is very small and as it is near to the resolution of the technique in air, the measurement of this value is not reliable. Above the charge region, it is due to the additional potential V_q produced by the trapped charges.

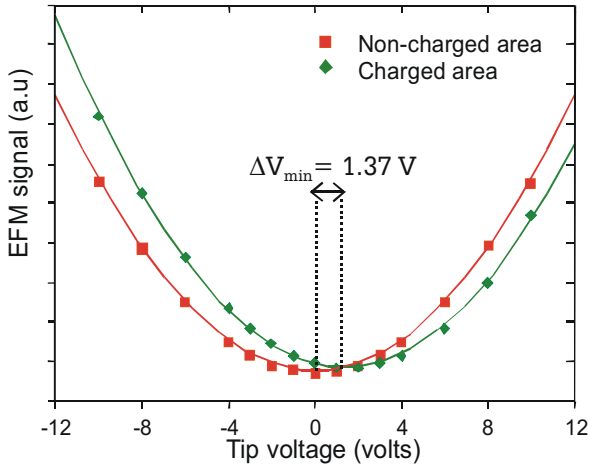


Figure 6: EFM phase signal in function of the tip-sample voltage (V_{EFM}) at $z_0=300\text{nm}$ for charged and uncharged regions. The two curves do not have the same minimum.

As the phase is proportional to the force gradient, they reached their minimum for the same value of V_{EFMmin} then the calculation of q is straightforward:

$$(17) F'(z_0) = 0 \text{ for } q = \frac{\epsilon_0 \epsilon_{\text{SiO}_2} S}{d} (V_{\text{EFMmin}} - V_C)$$

In the figure 6, the phase is minimal above the charged region when V_{EFM} equal 1.37V leading to a number of 1500 trapped charges. For this estimation an oxide layer thickness of 25nm and an effective tip area of $1.26 \times 10^5 \text{ nm}^2$ (400nm diameter disc) have been used. The effective tip area is large because the phase signal has been recorded at an altitude of 300nm.

There is one more method to quantify the trapped charge, which is based on the approach-

retract curves in dynamics mode [30]. This method is not explained in this paper but it has been successfully used to study the static charge distribution in an individual single-walled carbon nanotube [31].

Now that the method of charge quantification is established, the next challenge is to determine the spatial and charge resolutions of the EFM technique.

5 Spatial and charge resolutions of EFM

In EFM like in AFM, there is the lateral and the vertical resolution. At room temperature, the Brownian motion due to the thermal noise limits the vertical resolution because it induces an oscillating movement of the cantilever. This permanent movement fixes the minimum value of the force gradient that the system can measure [32]:

$$(18) \left. \frac{\partial F}{\partial z} \right|_{\min} = \frac{1}{A_0} \sqrt{\frac{27k_B T B k}{\omega_0 Q}}$$

where A_0 is the oscillating amplitude, k_B is the Boltzman constant, T is the temperature, k the cantilever stiffness, B is the bandwidth, ω_0 the resonance frequency and Q the quality factor. At room temperature $k_B T = 26\text{meV}$, for a cantilever with a resonance frequency of 100kHz and an oscillating amplitude $A_0 = 20\text{nm}$ and a bandwidth of 300Hz, the force gradient of the thermal noise $(\partial F / \partial z)_{\min}$ is about 2.10^{-3} N/m . The combination of equations (14) and (16) leads to a minimum number of trapped charge q_{\min} :

$$(19) q_{\min} = \sqrt{\frac{F'_{\min} \left(z_0 + \frac{d}{\epsilon_{\text{SiO}_2}} \right)^3 \epsilon_0 \epsilon_{\text{SiO}_2}^2 S}{d^2}}$$

For a 25nm silicon oxide layer, a z_0 tip-surface distance of 50nm leading to an effective tip-surface area of interaction S of 6260nm^2 , a minimum number of charge of about 20 is found. To improve this charge threshold a solution is to work at low temperature; the second one is to work in ultra high vacuum where the quality factor Q is improve at least by a factor of 100.

In EFM, the lateral resolution defines the capability of the technique to detect independently two separated electric charges. In the model of electrostatic gate [33] a line of electrical charges separated by a distance a , produces an electric field. It has been calculated that the electric field becomes uniform for an altitude $z \geq a$. If we reverse the situation: during the electrical mapping, the tip is lifted around 50nm then two charges could be imaged independently if they are separated by a minimum of 50nm. To improve the lateral resolution the tip-sample distance can be reduced but it should be kept in mind that when the tip is closed to the surface, it will probe the surface force at the same as the electrostatic one leading to altered measurements.

6 Study of space-time behavior of electric charges in Si nanostructures by EFM

The behavior of electric charge has been studied by EFM in three types of sample: the unconfined, the semi-confined and the confined samples. A layer of oxide on a conductive substrate is an unconfined sample because the injected charge are free to propagate in all the volume or surface of the layer. During the last ten years, this type of sample has been intensively studied in order to determine if the charges are trapped in volume and/or surface [34, 35] and how they evacuate. A recent work using EFM to record the space-time evolution of the charges in a silicon oxide layer [8], demonstrated that two main mechanisms are involved: the ohmic conduction thanks to the coulombic repulsive force and the diffusion at the surface according to a Fick law.

Conductive quantum dots with a size less than 10nm embedded in an oxide layer deposited on a conductive substrate is a semi-confined sample because the injected charge can propagate in the volume or surface under certain energy conditions. Indeed several studies [5,6,7] have demonstrated that the quantum dots act as powerful traps with a limited number of charges per dot. A mechanism based on Coulomb blockade effect [15] governs the charge propagation in link with the quantum dots distribution in the oxide layer [36].

For confined samples as individual conductive nano-structures deposited on an oxide layer, few studies have been carried out at room temperature [9, 10, 29]. However, such structures have a great interest because the injected charges are constrained to propagate and interact in a finite geometry. To characterise charge behaviour in such environment, monocrystalline silicon nanostructures supported on a silicon oxide layer of thickness d on top of a silicon substrate have been charged by the AFM tip. The nanostructures are covered by a thin layer of silicon oxide (2nm) as illustrate in figures 7 where two nanostructures geometry are presented: a rectangular one with of 15nm in height and 75nm in width and a ramified one, both supported on 7nm or 400nm oxide layer. These structures have been fabricated from SOI sample using FIB (Focus Ion Beam) to insulate the resin before the lift off process. The ramified structures have been obtained during an unexpected spreading of the resin; nevertheless this sample has been very useful for studying charge propagation. After this patterning step, the structures are covered by a thin layer of silicon oxide (2nm). Two qualities of oxide were used: a High Temperature Oxide (HTO) and a Rapid Temperature Oxide (RTO). The HTO exhibits a high concentration of defect while the RTO a low one.

Subsequent experimental issues will be at least twofold: i) a better understanding of the influence of the oxide layer thickness in the injection and detection process; ii) the investigation of the charge localisation and dynamics in function of structure geometry and quality of the covered oxide.

The top of the figure 8 represents the sample 1 that consists of several individual rectangular nano-structures deposited on a 7nm oxide layer while the bottom of figure 8 represents the sample 2 that consists of similar rectangular nano-structures deposited on 400nm oxide layer. The lateral separation between two rectangular dots is 225nm. For each sample an individual nano-structure have been charged using the same injection parameters (10V; 10s). In both cases, the EFM image exhibits a phase shift of 2 degrees. For a constant phase shift and $z_0=50\text{nm}$, q_2 can be straightforward calculate from equation (15) but to calculate q_1 , the dot height (17nm) must be taken into account leading to the following expression:

$$(20) \quad q_1 = \sqrt{\frac{\Delta\phi \times k \left(z_0 + \frac{d}{\epsilon_{\text{SiO}_2}} + \frac{d_1}{\epsilon_{\text{Si}}} \right) \epsilon_0 S}{Q \left(\frac{d}{\epsilon_{\text{SiO}_2}} + \frac{d_1}{\epsilon_{\text{Si}}} \right)}}$$

From the q_1 and q_2 values, a charge ratio (q_1/q_2) of 7 is found, which means: i) There is seven times less of injected charge in the dot of sample 2 (thick oxide layer) than in the dot of sample 1; ii) The minimal number of charge that the EFM technique can detect, relies on the oxide thickness.

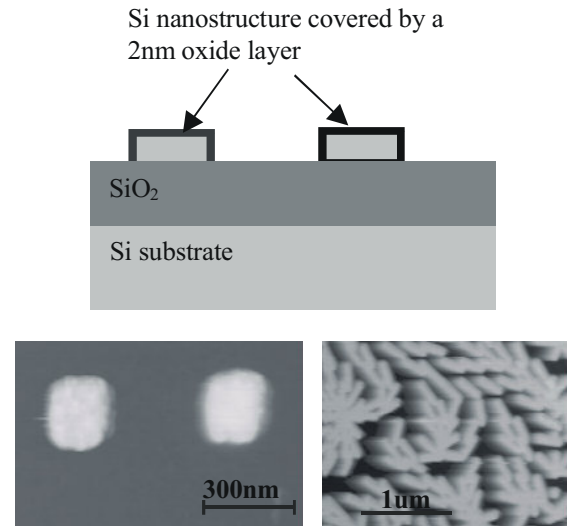


Figure 7: Top: vertical sample geometry: Si nanostructures covered by an 2nm oxide layer supported on an d oxide layer deposited on silicon substrate; Bottom left: sample 1 geometry: rectangular nanodot; Bottom right: sample 2 geometry: ramified nanostructure.

At the light of these results, the electric field appears as a key parameter in the injection process. Experiments have been realised to determine the electric field threshold needed to inject the minimum value of charge above the one the EFM technique is able to detect. On the sample 1 (thin oxide layer), five nanostructures have been charged using five different voltages (-2V, -3V, -4V, -5V and -6V) for 10s. For the voltages between -2V and -5V, a very small phase shift is detected on the EFM image (figure 9); this shift is so small that it falls down the detection limit of the technique in air.

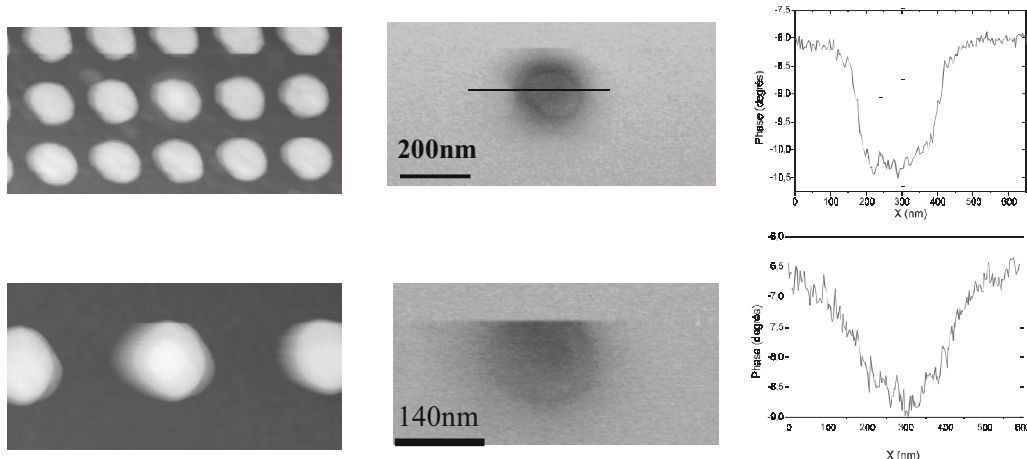


Figure 8: Influence of oxide thickness on nanostructure charging. Injection parameters $-8V/10s$. Top: sample 1 with 7nm of oxide layer. Left: topography image; center: EFM image; right: phase cross section. Bottom: sample 2 with 400nm of oxide layer; left: topography image; center: EFM phase image; right: phase cross section

On the other hand, for $(-6V)$ a phase shift of 1 degree is measured leading to estimate the electric field threshold about $2.5 \times 10^8 V/m$. This threshold is rather surprising since this value is one order of magnitude higher than the one needed to inject charge in nanostructure on a thick layer of oxide. Nevertheless this injection threshold is relative to the detection one, which is dependent of the oxide layer thickness (i.e. equation 15). In fact it can not be assumed that no charge are injected for voltage lower than $|-6V|$, to solve this question, similar measurement have to be carried out on ultra high vacuum where the force gradient resolution is improved.

To localise where the charges are trapped, injection experiments have been performed into a ramified Si structure supported on 7nm-oxide layer and covered by 2nm of HTO. The injection takes place at the middle of the structure by applying 10V for 10s. In Figure 10, the charged region is easily distinguished to the uncharged ones because it exhibits a homogenous phase signal in all it. This homogenous signal is the signature of the charge propagation in all the structure. This observation demonstrates that the silicon nanostructure behaves like a metal and becomes iso-potential.

When the silicon ramified structure is covered by a 2nm RTO layer, as the figure 11, a larger phase shift appears at the injection point compared to the rest of the structure. This specific spot does not present the same time dependence that the charges in the nanostructure. Indeed after several minutes, this spot is still visible in EFM image while the silicon charge is gone. This result demonstrates that the charges are trapped differently and are localised in the RTO layer. In the case of a HTO layer, this effect is not observed. The high level of defects in HTO layer compared to RTO one can explained the origin of this difference by making easier the recombination of the charges.

The last issue to address through these experiments is the temporal evolution of the charges

in such confined structure and how they interact. When electric charges are confined in small nanostructure, their density is high and creates a strong repulsive effect between the charges. If we consider that 100 electrons are confined in a dot of 100nm in diameter, the charge density is $10^{17} cm^{-3}$. In this configuration, the electrons are trying to get out of the dot but the oxide layer prevents their escape. In order to illustrate this repulsive effect, the following experience has been realised: after a charge injection of 10V/10s in a rectangular dot, the tip is grounded and put in contact with the charged dot for 10s. The result of this experiment is presented in figure 12. Between the top of the EFM image (fig 12) recorded before the tip contact, and the bottom recorded after, a phase signal decrease about 0.5 degree is measured. This indicates that some charges have been removed from the dot, they passed through the 2nm-oxide cover to reach the tip. This means that the voltage difference between the grounded tip and the dot is high, probably several hundred of mV for allowing tunneling effect. Step by step when the charges are tunneling through the oxide, the dot potential diminishes until the tunneling probability becomes negligible. As the tunneling time of the charges can be negligible (10^{-14} to 10^{-12} s) compared to the 10s of tip-dot contact, the limited factor is then the tip-dot voltage decrease explaining why there are still some charges in the dot after 10s.

The confinement of a great number of electric charge in small volume, produces a high electrostatic energy E_C that should overcome the others energies at room and low temperatures. This expression of E_C is:

$$(21) E_C = \frac{1}{2} \frac{q^2}{C} \text{ where } q \text{ is the total charge and } C \text{ is the capacitance of the Si dot}$$

To calculate C , we approximate the rectangular dot by a sphere with a radius R covered by an oxide layer. The value of R is adjusted to obtain a sphere volume equal to the dot volume of $10^{-20} m^3$. If we consider that 100 charges (low estimation) are present in the dot, a repulsive Coulombic energy of 130meV per charge is found. This energy is far higher than the thermal one (26meV at room temperature). In this energy configuration, we could suppose that the charge formed a Wigner crystal in the nano-dot.

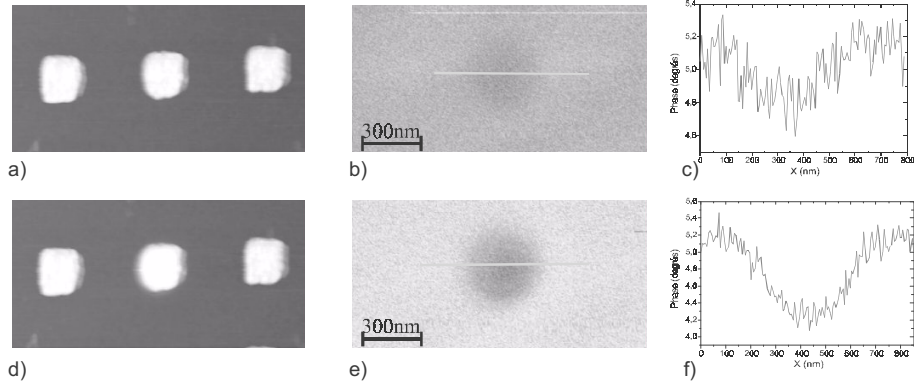


Figure 9: Electric field threshold for injection. Top: injection parameters $-5V/10s$. a) Topography image; b) EFM signal; c) Phase cross section. Bottom: injection parameters : $-6V/10s$. d) Topography image; e) EFM phase image; f) Phase cross section

The distribution of individual charge in an organised crystal, called Wigner crystal, has been observed at low temperature for quantum systems when the electronic density is low [37]. In that case, the Coulombic repulsive force between the charges becomes far higher than the thermal one leading to the distribution of charges on a grating to minimise the interaction energy. This effect verified by Monte Carlo simulation, has never been observed experimentally on system contained a great number of electron. To validate this hypothesis, similar experiment should be carried on vacuum and at low temperature where EFM technique is more accurate and has a greater resolution in charge detection.

The strong Coulombic repulsive effect leads to another phenomenon: the evacuation of the charge from the nanostructure. Indeed in figure 12 we observe that the charges trapped in the nanostructure disappears after 30mins. The charge evacuation is homogenous which indicates that there is no preferential path. The mechanism is not well understood and it may occur by charge diffusion through the oxide traps according to Fick law and/or ohmic conduction [8].

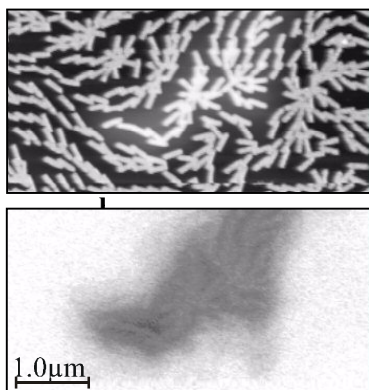


Figure 10: Charge propagation in ramified nanostructure. Injection at the middle on the structure by applying $(-10V/10s)$. a) Topography image; b) EFM phase image. Z phase scale: $[0-10]$ degree

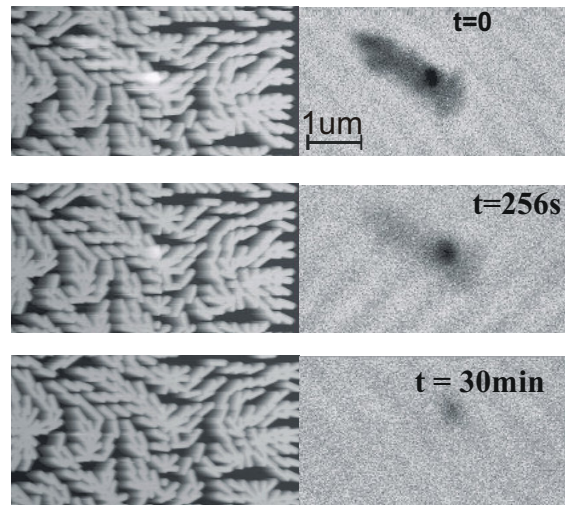


Figure 11: Time evolution of injected charges in ramified nanostructure covered by a 2nm RTO layer. At the injection point $(-7V/10s)$, the EFM phase signal is higher than in the rest of the structure.

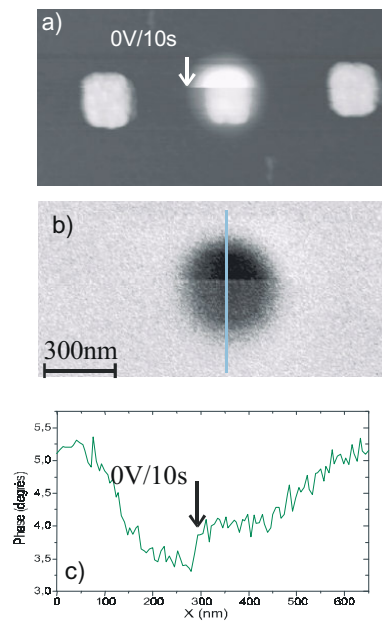


Figure 12: Discharge experiment: the tip is grounded and comes in contact to the charged dot during 10s. a) Topography image; b) EFM Phase image; c) Phase cross section.

7 Conclusion

A linear treatment of the oscillating cantilever movement probing a long-range force potential is sufficient for explaining EFM technique in classic image mode for lift height in the [50-300]nm. Thanks to this treatment, a simple relation between the phase the force gradient and the tip-surface voltage, is found. A qualitative analysis of this relation leads to three possible configurations of EFM phase shift according to the tip polarisation and sign of trapped charge. This analysis gives a clear interpretation of “bump” or “hole” apparition in EFM image. Analytic calculation of the metallic tip-sample capacitances and their force gradients was carried out to quantify trapped charge from phase shift measurements in EFM image mode or voltage spectroscopy. Next the spatial and charge resolution of the EFM technique have been treated. It has been underlines that the charge resolution is limited by the thermal noise, leading to a detection threshold at room temperature of about 20 for trapped charges in a 25nm-silicon oxide layer. On the other hand, using the model of electrostatic gate, it has been found that the lateral resolution is dependent of the lift height: the tip can detect individually two charges if there are separated by a distance equal to the lift height.

Finally, charge injection experiments were carried out on individual silicon nanostructures to correlate: the charging level with the oxide thickness that supports the nanostructures, the charge localisation with the quality of the cover oxide, the dynamics of the charge propagation and distribution with the structure geometry.

In the same injection conditions, experiments have shown that the charging level is seven time higher for dots supported by 7nm-oxide layer than for the ones on a 400nm-oxide layer. This result highlights the electric field as a key parameter in the injection mechanism. By performing injections in silicon dot covered by a HTO layer and on dot covered by RTO layer, it has be determined that charge are trapped mainly in the silicon dot rather than the oxide layer. Injection experiments in ramified nanostructures have demonstrated that the charges propagate in all the structure leading to a homogenous charge distribution. From this charge behaviour, we can conclude that such silicon nanostructures act as a metal. However, further experiments should be carried out to validate the formation of a Wigner crystal in such nanostructure.

REFERENCES

[1] J. Lambert and al, 2003, J. Appl. Phys. vol 93, 5369
[2] K. Domansky and al, 1993, Appl. Phys. Lett vol 63, 1513
[3] K. Kimura and al, 2003, Appl. Surf. Sci, vol 230, 93
[4] M. Nonnenmacher, 1991, Appl. Phys. Lett vol58, 2921
[5] D. Schaadt and al, 1999, Appl. Phys. Lett vol 74,472

[6] C. Guillemot and al, 2002, Europhys. Lett., vol 59, 566
[7] C. Y. Ng and al, 2004, Appl. Phys. Lett., vol 85, 2941
[8] G. Bush and al, 2001, Appl. Phys. Lett., vol 79, 2010
[9] T. Melin and al, 2002, Appl. Phys. Lett., vol 81, 5054
[10] M.J. Gordon and T. Barom, Phys. Rev. B, vol 72, 165420
[11] H. Fan and al, 2004, Science 304, 567
[12] H. Graf and al, 2002, Appl. Phys. Lett., vol 80, 1264
[13] L. Klein and al, 2001, Appl. Phys. Lett., vol 79, 1828
[14] E. Bussman and al, 2004, Appl. Phys. Lett., vol 85, 2538
[15] K. K. Likharev, 1999, Proc. IEEE 87, 606
[16] A. Nakakima and al, 2002, Appl. Phys. Lett., vol 81, 733
[17] M. Mizuta and al, 2001, Nanotechnology, vol 12, 155
[18] F. Marchi and al, 1998, J. Vac. Sci. Technol. B 16, 2952
[19] P. Avouris, 1997, Appl. Phys. Lett., vol 71, 285
[20] B. Bhusban and al, 2004, *Handbook of Nanotechnology* Springer press
[21] S. Sarid, 1994, *Scanning Force Microscopy*, New York: Oxford University Press
[22] S. Jeffrey and al, 2000, Appl. Surf. Sci. 157, 280
[23] J. Colchero and al, 2001, Phys. Rev B 64, 245403
[24] L. Klein and al, 2000, Appl. Phys. Lett., 77, 3615
[25] C. H. Lei and al, 2004, Nanotechnology 15, 627
[26] S. Hudlet and al, 1998, Eur. Phys. J. B 2,5
[27] E. Durand, *Electrostatique*, vol II, Masson et Cie (1966)
[28] B. Terris and al, 1989, Phys. Rev. Lett., vol 63, 2669
[29] T. Melin and al, 2004, Phys. Rev. B, 69, 035321
[30] R. Dianoux and al, 2003, Phys. Rev. B, 68, 045403
[31] M. Paillet and al, 2005, Phys. Rev. Lett, 94, 186801
[32] Y. Martin and al, 1987, J. Appl. Phys, 61, 4723
[33] R. Feynman and al, 1977, The Feynman lectures on physics, vol II. Addison Wesley Publishing Company, Reading (MA)
[34] J. Lambert and al, 2002, J. Apply. Phys., vol 91, 9161
[35] N. Felidj and al, 2000, Europhys.Phys. J. 12, 85
[36] R. Dianoux and al, 2005, Phys. Rev B, vol 71, 125303
[37] A. Filinov and al, 2001, Phys. Rev. Lett., vol 86, 3851